

Analysis and Simulation of Misalignment Issues in Dynamic Wireless Charging for Electric Vehicles



Kundan Kumar and Ngangoiba Maisnam

1 Introduction

The emerging technologies in the energy and transportation sectors, such as electric vehicles, provide several advantages in terms of the economy and environment-friendly. The charging technology of an EV during the motion can be defined as dynamic wireless charging (DWC). With the help of DWC technology, various challenges may be resolved such as the volume of the battery and the inability to drive EVs over long distances [1]. The designing of transmitting coils and their configurations are very much important for the smooth charging of various types of electric vehicles maintaining higher efficiency [2].

The researchers have used various topologies to study the misalignment of the DWC system. A technique for constructing a transmitting coil utilizing a compensation network has been presented by S. Li et al. in consideration of transfer performance, electrical stress, and zero voltage switching (ZVS) [2]. The coupling coefficient and self-inductance calculations are presented by Sampath et al. using the finite element method (FEM). Furthermore, an optimization methodology against misalignment for DWC is discussed [3]. A three-dimensional analytical rectangular coil model has been proposed by Kushwaha et al. for computing mutual inductance for various misalignments [4]. This paper introduces a 3-D model of a circular helix coil for both transmitting (T_x) and receiving (R_x) coils. Both the T_x and R_x coils are placed in an air medium.

Further, analysis to get comparable findings in accordance with mutual inductance, magnetic flux, and coupling coefficient, k , is presented with various measurements along the y-axis (longitudinal distance) and z-axis (vertical distance), i.e., air-gap distance.

K. Kumar (✉) · N. Maisnam
National Institute of Technology Manipur, Imphal 795004, India
e-mail: kundankumar.nitm@gmail.com

In this paper, misalignment issues of DWC for an EV are analyzed and simulated. The overview of the DWC system and its working are described in Sect. 2. The significance of coupling pads and misalignment are discussed in Sect. 3. The simulation analysis and various results for modeled coil structures are presented in Sect. 4. The summary of the paper is concluded in Sect. 5.

2 Overview of DWC and Its Working

The DWC system is the present demand for EV technology which strengthens the charging infrastructures. In the DWC system, the vehicle battery can be charged even though it is in motion. It is important to give attention to a multi-objective design strategy for the DWC system that takes into account both the coupling coils and the compensation networks. When designing a DWC system, the LCC network is employed as a compensation network to achieve constant output current and zero voltage switching (ZVS) conditions [2].

Figure 1 exhibits the DWC system's schematic representation. N transmitting coils comprise the system, and each coil has dimensions of length (L_x) and width (B_x) (whereas $x = 1, 2, \dots, N$). The W is the distance between two consecutive transmitting coils. L is the overall length of N coils including distances between consecutive transmitting coils. There is a single receiving coil placed on the vehicle denoted by k which is shown in Fig. 1 by the red periphery. The LCC compensation network is used to account for the reactive components of a single transmitting coil. To adjust the power-supplying coils, N number of switches (S_1, S_2, \dots, S_N) are connected with the LCC networks and the high-frequency inverters. The detecting devices, i.e., sensors, are installed beside each transmitting coil to locate the exact position of the receiving coil. The activation and deactivation of each transmitter coil can be managed with the help of artificial intelligence (AI) techniques. However, the detection and sensing control are not included in this work.

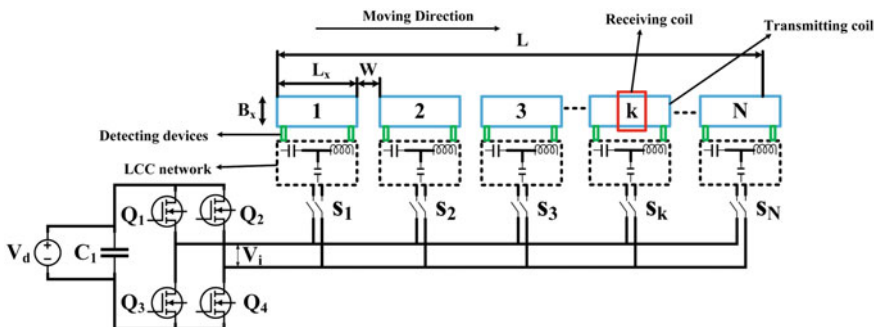


Fig. 1 Dynamic wireless charging (DWC) system

For simplicity, two transmitting coils (T_x) and one receiving coil (R_x) system are considered in this study and the circuit diagram is given in Fig. 2. The LCC network is employed in Fig. 2, where L_{mT_1} and R_1 are the transmitting coil 1's inductance and resistance, respectively, whereas for the transmitting coil 2 inductance and resistance can be termed as L_{mT_2} , and R_2 , respectively. On the other hand, the inductance and resistance of the receiving coil are represented by L_R and R_R , respectively. The input impedances of transmitting coils 1 and 2 are denoted by Z_1 and Z_2 , respectively, while for the receiving coil Z_R . The load impedance of receiving side is denoted by Z_L . The different values of the LCC network can be estimated by the following formula.

$$L_{mT_n} = \frac{X_T}{\omega} \tag{1}$$

$$C_{TT_n} = \frac{1}{\omega X_T} \tag{2}$$

$$C_{TR_n} = \frac{1}{(\omega L_{T_n} - X_T)}, \tag{3}$$

Where ω is the angular frequency, X_T is the equivalent impedance of the transmitting coil, L_{mT_n} is the self-inductance of the transmitting coil (where $n = 1$ and 2), C_{TT_n} and C_{TR_n} is the capacitance of the transmitting coil (where $n = 1$ and 2). The high-frequency inverter (HFI) output voltage is denoted by V_i which is fed to transmitting coils and the transmitting current by I_n (where $n = 1$ and 2), then X_T is given by

$$X_T = \frac{V_i}{I_n} \tag{4}$$

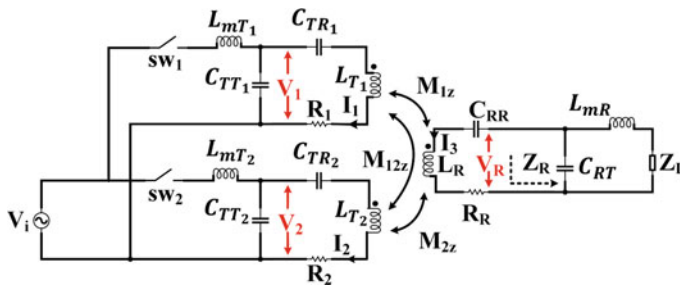


Fig. 2 Circuit diagram of the DWC system

2.1 Operation of the DWC System

The HFI is connected to both the transmitting coils, and activation of both the transmitting coils is maintained by turning on and off the switches sw_1 and sw_2 [2, 3]. The operation of the segmented DWC system is categorized into three stages which are given as follows.

STAGE 1: $sw_1 = \text{ON}$, $sw_2 = \text{OFF}$.

In this stage, the system's KVL equation is expressed in matrix form as given by,

$$\begin{bmatrix} Z_1 & j\omega M_{12z} & j\omega M_{1z} \\ j\omega M_{12z} & Z_2 - jX_T & j\omega M_{2z} \\ j\omega M_{1z} & j\omega M_{2z} & Z_R \end{bmatrix} \begin{bmatrix} I_1 \\ I_2 \\ I_3 \end{bmatrix} = \begin{bmatrix} V_1 \\ 0 \\ 0 \end{bmatrix}, \quad (5)$$

where the mutual inductances M_{1z} and M_{2z} are those between T_x coil 1 and R_x coil and between T_x coil 2 and R_x coil, respectively. The mutual inductance of both the T_x coils is M_{12z} . The currents flowing through the T_x and R_x coils are

$$I_1 = \frac{V_s}{jX_T} \quad (6)$$

$$I_2 = -I_1 \cdot \frac{\omega^2 M_{12z} M_{2z} + j\omega M_{12z} Z_R}{\omega^2 M_{2z}^2 + (Z_2 - jX_T) Z_R} \quad (7)$$

$$I_3 = \frac{j\omega(M_{1z} I_1 + M_{2z} I_2)}{Z_R}. \quad (8)$$

The voltage induced in the receiving coil is given by

$$V_R = \omega M_{1z} I_1 + \omega M_{2z} I_2 \quad (9)$$

STAGE 2: $sw_1 = \text{ON}$, $sw_2 = \text{ON}$.

In this stage, the system's KVL equation is expressed in matrix form as given by,

$$\begin{bmatrix} Z_1 & j\omega M_{12z} & j\omega M_{1z} \\ j\omega M_{12z} & Z_2 & j\omega M_{2z} \\ j\omega M_{1z} & j\omega M_{2z} & Z_R \end{bmatrix} \begin{bmatrix} I_1 \\ I_2 \\ I_3 \end{bmatrix} = \begin{bmatrix} V_1 \\ V_2 \\ 0 \end{bmatrix}. \quad (10)$$

The currents of transmitting and receiving coils are given by

$$I_1 = \frac{V_s}{jX_T} \quad (11)$$

$$I_2 = \frac{V_s}{jX_T} \quad (12)$$

$$I_3 = \frac{j\omega(M_{1z}I_1 + M_{2z}I_2)}{Z_R} \quad (13)$$

The receiving coil's induced voltage can be represented by (9).

STAGE 3: $sw_1 = \text{OFF}$, $sw_2 = \text{ON}$.

Similarly, for the third stage, the above analysis can be carried out by exchanging the subscripts "1" and "2."

3 Coupling Pad and Misalignment

The most crucial component of the DWC system is the coupling pads. For coupling pads, it is important to have high-quality factor Q , high misalignment tolerance, and high coupling coefficient k [5–10].

The above-said parameters depend on the inductor's shape, core material, and spacing between the coils (i.e., T_x and R_x coils) [6–8]. The efficiency of linked inductors in a DWC system depends upon the inductor's quality factor and magnetic coupling coefficient. The geometric average of the transmitter and receiver quality factor denoted as Q is given as:

$$Q = \sqrt{Q_T Q_R} \quad (14)$$

$$Q_T = \frac{\omega L_T}{R_T} \quad (15)$$

$$Q_R = \frac{\omega L_R}{R_R}, \quad (16)$$

where Q_T and Q_R represent the transmitting and receiving coil quality factors, respectively. The equivalent inductance of the T_x and R_x coils is L_T and L_R , respectively (where $T = 1$ and 2). The equivalent resistance of the T_x and R_x coils is termed R_T and R_R , respectively (where $T = 1$ and 2).

It is necessary to design the inductor with a high level of self-inductance, low series resistance, and a relatively high frequency to get a high Q [9]. So, lowering the coil's resistance is necessary to raise Q . The value of coil self-inductance can be computed by (17) [7].

$$L = \frac{\mu N^2 A}{l}, \quad (17)$$

where l is the mean length, N is the number of turns, A is the conductor's cross-sectional area, and μ represents the flux path's magnetic permeability.

3.1 Circular Helix Coil

The parameters considered for designing the DWC system are shown in Table 1. Figure 3 shows the model representation of the circular helix coil, where the coil's dimensions are shown in Fig. 3a, and a 3-D representation of the coil's circular helix is presented in Fig. 3b. The transmitter (T_x) coil is presented in blue color, and the receiver (R_x) coil is in red color that is physically spaced by an air gap. The transmitter coil is energized by the HFI current, whereas the receiver coil is not connected to any active sources. Power is transferred in the DWC system via a magnetic field that the transmitting coil generates and couples to the receiving coil via an air medium. A magnetic connection between coils is necessary for the DWC system to transfer the power maintaining optimum efficiency [11–13]. The orientation and the flux linkage of the coils affect the performance of the DWC system [14].

Table 1 Design specification of circular helix coil

Sl. no.	Parameters	Values	Unit
1	Wire radius	3	mm
2	Start helix coil radius	40	mm
3	No. of turns	3	
4	Current	5	A
5	Coil pitch	8.01	
6	Terminal coil diameter	2	mm
7	Terminal coil length	500	mm

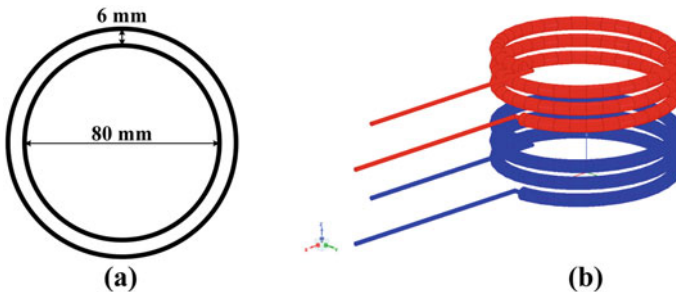


Fig. 3 Model representation **a** dimension of circular helix coil, and **b** 3-D geometry of circular helix coil

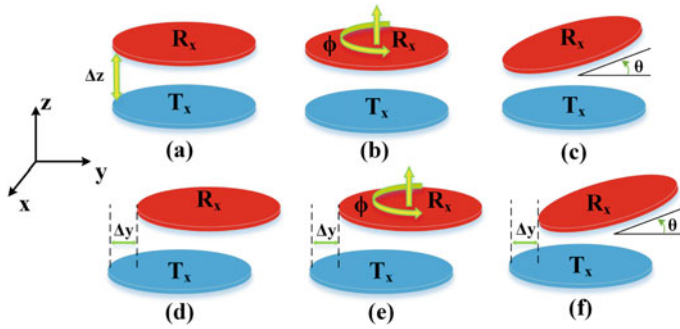


Fig. 4 Various types of misalignments **a** vertical, **b** planar, **c** angular, **d** longitudinal, **e** planar and longitudinal, and **f** angular and longitudinal [14]

3.2 Misalignment

The various types of misalignment are shown in Fig. 4. It can be observed that due to different diverse positions of the receiving (R_x) coil, different misalignments can categorize such as vertical, planar, angular, longitudinal, planar and longitudinal, and angular and longitudinal [4]. If the receiving coil moves in the vertical direction, then the deviation is represented by Δz and is called vertical misalignment as shown in Fig. 4a. In case of planer misalignment, the receiving coil is rotated with an angle ϕ (i.e. $0 < \phi \leq 2\pi$) parallel to the transmitting coil at a fixed center with constant height as shown in Fig. 4b. In Fig. 4c, the receiving coil deviates at an angle θ (where $0 < \theta \leq \pi$) by maintaining the same center point by both the T_x and R_x coils without any vertical misalignment which is named as angular misalignment [15–17]. When the receiving coil travels along the longitudinal direction, several sorts of variations are conceivable. In this kind of misalignment, the T_x and R_x coil’s centers are displaced by Δy in the y-direction, as shown in Figs. 4d–f. The receiving coil is misaligned longitudinally in Fig. 4d when it is shifted in the y-axis with a constant height. The receiving coil in Fig. 4e is shifted in the y-axis and rotated at a fixed height, which is referred to as planar and longitudinal misalignment. In the case of angular and longitudinal misalignment, the receiving coil is deviated by an angle θ and displaced in the y-axis as shown in Fig. 4f [16].

4 Simulation Analysis and Result Discussion

The simulation studies are carried out by considering one transmitter coil as well as one receiver coil to observe the misalignment of the DWC system. ANSYS MAXWELL 3-D is used to validate the specified analytical model. Both the coils (i.e., T_x and R_x) have been simulated with the consideration of an air-gap distance of

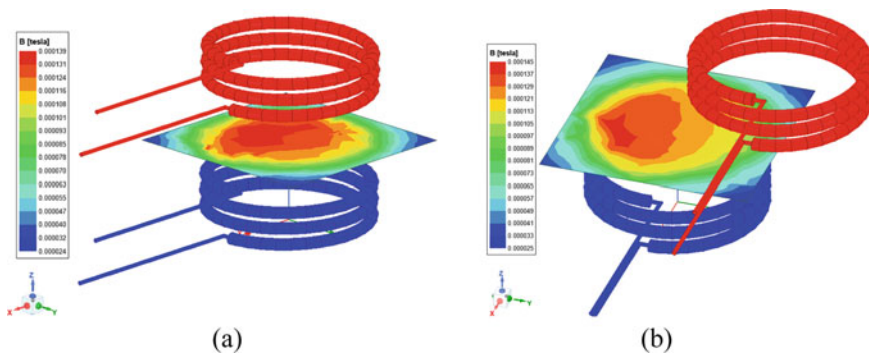


Fig. 5 Magnetic field density between T_x and R_x with the variation of **a** 0 mm y-axis and 65 mm z-axis. **b** 50 mm y-axis and 65 mm z-axis

65 mm on the z-axis (vertical) while in the y-axis (longitudinal) distance is considered as 0 and 50 mm which are displayed in Fig. 5a, b, respectively. Figure 5 also depicts the magnetic field density between the transmitter and receiver coils. The highest magnetic density is observed in the heated region, which is represented by the red zone in Fig. 5a, with a value of 0.000139 T (Tesla) at an air-gap (vertical) distance of 65 mm in the z-axis and no fluctuation in the y-axis, while the lowest is observed in the blue zone, with a value of 0.000024 T (Tesla). Likewise, the hot region in Fig. 5b exhibits the highest magnetic density at an air-gap (vertical) distance of 65 mm on the z-axis and a misalignment of 50 mm on the y-axis, with a value of 0.000145 T (Tesla) and the value of the lowest zone, blue, is 0.000025 T (Tesla). Examining Fig. 5a, b shows a difference of 0.000006 T.

Further, in the event of a vertical variation, the receiving coil shifts along the z-axis, while they move along the y-axis when there is a longitudinal misalignment. By changing the z-axis and y-axis distances, several values are simulated in accordance with the mutual inductance, flux linkage, magnetic field density, and coupling coefficient.

The parameters of the considered analytical model are used to observe the coupling coefficient, mutual inductance, and magnetic flux density of different variations in the y-axis (longitudinal distance) and z-axis (vertical distance) [18, 19]. The coupling coefficient k of transmitting coil input (T_{x_in}) and receiving coil input (R_{x_in}) is shown in Fig. 6. As the distance between the coils rises, the value of k decreases. Multiple results were computed for different variations in the y-axis for a significant distance in the z-axis. The coupling coefficient is shown by the red curve at an air-gap (vertical) distance of 35 mm for the variations in the y-axis, the green curve at an air-gap (vertical) distance of 45 mm, the blue curve at an air-gap (vertical) distance of 55 mm, and the orange curve at an air-gap (vertical) distance of 65 mm.

It is observed that the self-induced flux on the transmitting coil is constant while the flux linkage is varying along with the movement of receiving coil as shown in Fig. 7.

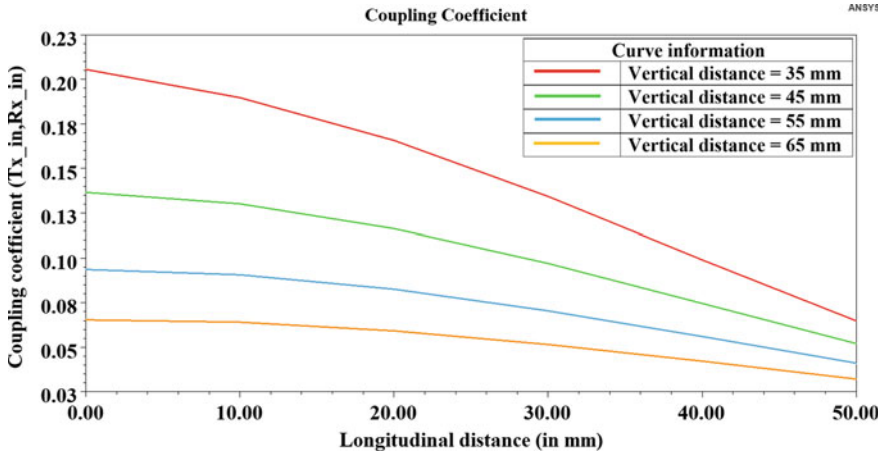


Fig. 6 Coupling coefficient of T_{x_in} and R_{x_in}

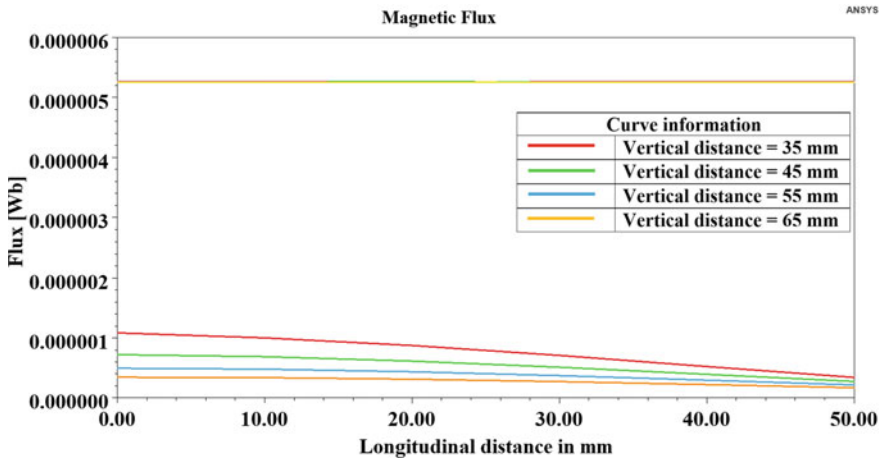


Fig. 7 Flux linkage in T_x and R_x coils

The red curve indicates the flux in the receiving coil at a 35 mm air-gap (vertical) distance and varies along the longitudinal axis. The green curve, which varies along the longitudinal axis, depicts the flux in the receiving coil at a 45 mm air-gap (vertical) distance. The blue curve, which varies along the longitudinal axis, depicts the flux in the receiving coil at a 55 mm vertical (air-gap) distance. The orange curve, with changes in the longitudinal axis, depicts the flux in the receiving coil at a 65 mm vertical (air-gap) distance. In Table 2, different values of mutual inductance between the T_x and R_x coils are surmised for divergence in the receiving coil. The mutual inductance value is decreasing as the R_x coils travel away from the T_x coil [20–23]. The visual representation of the mutual inductance between the T_x and R_x coils is

Table 2 Mutual inductance between T_x and R_x coil

Sl. no.	y-axis [mm]	M [nH] (for z = 35 mm)	M [nH] (for z = 45 mm)	M [nH] (for z = 55 mm)	M [nH] (for z = 65 mm)
1	0.00	216.84	144.20	98.89	69.02
2	10.00	200.16	193.55	95.87	67.63
3	20.00	174.81	122.75	87.25	62.51
4	30.00	141.73	102.34	74.39	54.41
5	40.00	104.60	78.66	59.19	44.52
6	50.00	68.33	54.88	43.36	33.93

y-axis: longitudinal distance, z-axis: air-gap distance (i.e. vertical distance), and M: mutual inductance between T_x and R_x

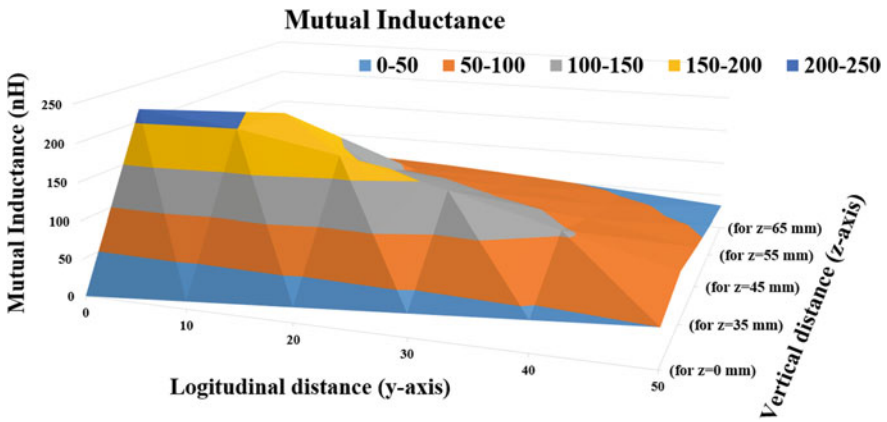


Fig. 8 Graphical view of mutual inductance

shown in Fig. 8. The graph clearly demonstrates that the mutual inductance values reflect the distance between the coils.

5 Conclusion

In this paper, the misalignment issues that arise in dynamic wireless charging (DWC) are investigated in detail. The impact of the DWC system and its working with the consideration of coupling coefficients, flux linkage, as well as mutual inductance are discussed. A circular helix coil is considered for analyzing the DWC system, and hence, an ANSYS MAXWELL 3-D model is created. The copper material is chosen for both the coils (T_x and R_x) and placed in an air medium for the simulation modeling. In the simulation studies, different misalignments are considered by varying the distances along the longitudinal and vertical, i.e., y-axis and z-axis, respectively,

and the variant in the mutual inductance, coupling coefficient, flux linkage, and distribution of magnetic flux density is observed. It is observed that the increase in deviation from the proper alignment leads to a decrease in mutual inductance, coupling coefficient as well flux linkage.

References

1. Patil D, McDonough MK, Miller JM, Fahimi B, Balsara PT (2018) Wireless power transfer for vehicular applications: overview and challenges. *IEEE Trans Transp Elect* 4(1):3–37
2. Li S, Wang L, Tao C, Li F, Wang L (2019) Designing of the transmitting coils and compensation network of a segmented DWPT system. In: 2019 IEEE 15th Brazilian Power Electronics Conference and 5th IEEE Southern Power Electronics Conference (COBEP/SPEC), pp 1–5
3. Sampath JPK, Alphones A, Vilathgamuwa DM (2016) Coil optimization against misalignment for wireless power transfer. In: 2016 IEEE 2nd Annual Southern Power Electronics Conference (SPEC), pp 1–5
4. Kushwaha BK, Rituraj G, Kumar P (2017) 3-D analytical model for computation of mutual inductance for different misalignments with shielding in wireless power transfer system. *IEEE Trans Transp Elect* 3(2):332–342
5. Zaheer A, Covic GA, Kacprzak D (2014) A bipolar pad in a 10-kHz 300-W distributed IPT system for AGV applications. *IEEE Trans Ind Electron* 61(7):3288–3301
6. Covic GA, Kissin MLG, Kacprzak D, Clausen N, Hao H (2011) A bipolar primary pad topology for EV stationary charging and highway power by inductive coupling. In: Proc IEEE Energy Convers Congr Expo, Phoenix, AZ, USA, pp 1832–1838
7. Kim S, Covic GA, Boys JT (2017) Tripolar pad for inductive power transfer systems for EV charging. *IEEE Trans Power Electron* 32(7):5045–5057
8. Chowdary KV, Kumar K, Behera RK, Banerjee S (2020) Overview and analysis of various coil structures for dynamic wireless charging of electric vehicles. In: 2020 IEEE International Conference on Power Electronics, Smart Grid and Renewable Energy (PESGRE2020), pp 1–6
9. Kiani M, Jow U-M, Ghovanloo M (2011) Design and optimization of a 3-coil inductive link for efficient wireless power transmission. *IEEE Trans Biomed Circuits Syst* 5(6):579–591
10. Moon S, Kim B-C, Cho S-Y, Ahn C-H, Moon G-W (2014) Analysis and design of a wireless power transfer system with an intermediate coil for high efficiency. *IEEE Trans Ind Electron* 61(11):5861–5870
11. Lin FY, Carretero C, Covic C, Boys J (2016) Reduced order modelling of the coupling factor for varying sized pads used in wireless power transfer. *IEEE Trans Transport Elect* 99:1
12. Fotopoulou K, Flynn BW (2011) Wireless power transfer in loosely coupled links: Coil misalignment model. *IEEE Trans Magn* 47(2):416–430
13. Diep NT, Trung NK, Minh TT (2019) Power control in the dynamic wireless charging of electric vehicles. In: 2019 10th International Conference on Power Electronics and ECCE Asia (ICPE 2019 - ECCE Asia), pp 1–6
14. Abou Houran M, Yang X, Chen W (2018) Magnetically coupled resonance WPT: review of compensation topologies, resonator structures with misalignment, and EMI diagnostics. *Electronics* 7:296
15. Ramezani A, Narimani M (2019) High misalignment tolerant wireless charger designs for EV applications. *IEEE Transp Elect Conf Expo (ITEC) 2019*:1–5
16. Shin Y, Hwang K, Park J, Kim D, Ahn S (2019) Precise vehicle location detection method using a wireless power transfer (WPT) system. *IEEE Trans Veh Technol* 68(2):1167–1177
17. Ong A, Jayathathnage PKS, Cheong JH, Goh WL (2017) Transmitter pulsation control for dynamic wireless power transfer systems. *IEEE Trans Trans Elect* 3(2):418–426
18. Razu MRR et al (2021) Wireless charging of electric vehicle while driving. *IEEE Access* 9:157973–157983

19. Triviño A, Sánchez J, Delgado A (2022) Efficient methodology of the coil design for a dynamic wireless charger. *IEEE Access* 10:83368–83378
20. Chowdary KVSR, Kumar K (2022) Assessment of dynamic wireless charging system with the variation in mutual inductance. In: *Proc IEEE Indian Council International conference (INDICON-2022)*, Kochi, India, 24–26 November, pp 1–6
21. Kumar K, Chowdary KVSR, Nayak BK, Mali V (2022) Performance evaluation of dynamic wireless charging system with the speed of electric vehicles. In: *Proc IEEE Indian Council International conference (INDICON-2022)*, Kochi, India, 24–26 November, pp 1–6
22. Zhang X, Meng H, Wei B, Wang S, Yang Q (2019) Mutual inductance calculation for coils with misalignment in wireless power transfer. *J Eng* 2019:1041–1044
23. Kumar K, Chowdary KVSR, Mali V, Kumar RR (2021) Analysis of output power variation in dynamic wireless charging system for electric vehicles. In: *Proc of IEEE International Conference on Smart Technologies for Power, Energy and Control (STPEC 2021)*, Bilaspur, India, 19–22 December, pp 1–6